Mining, Metallurgy & Exploration (2022) 39:1061–1071
https://doi.org/10.1007/s42461-022-00583-3

Numerical Analysis of the Effect of Bedding Plane Strength on Laminated Roof Failure in Underground Entries Using Coupled FDM-DEM

Qingwen Shi[1] · **Brijes Mishra**[2]

Received: 14 November 2021 / Accepted: 6 March 2022 / Published online: 17 March 2022

Abstract

Numerical simulations have been used to investigate roof fall in the past decades. When compared to the continuum-based methods, the discrete element method has been well recognized for its excellent performance in simulating large strain problems and the fracturing processes in the rock mass. However, the discrete element method has its limitations. When simulating a large-scale problem, a large number of particles are required, which consumes significant computational resources. In the present study, a 3D numerical model coupled with the finite difference method (FDM) and the discrete element method (DEM) was created to simulate the laminated roof failure in an eastern coal mine in the USA. In the FDM-DEM coupled model, the laminated roof of the entry is represented by an assembly of bonded particles using PFC3D. The laminated roof is simulated by adding parallel discontinuities. The discontinuities are given certain stiffness and strength parameters in the model. The rest of the surrounding rock, including ribs and floor, is represented by continuum zones using FLAC3D. The strength of the discontinuities is varied sequentially and the fracturing of the laminated roof was analyzed with respect to entry advance. The results showed that the laminated roof fractures along the discontinuities, while an intact roof fractures in a dome shape. Increasing the strength of the discontinuity could enlarge the tensile zone inside the laminated roof and hence change the crack distribution. In addition, the number of cracks in the laminated roof behind the advancing face decreases with the increment of discontinuity strength while this trend is not occurring ahead of the advancing face. The simulation demonstrated that the coupled method using PFC3D/FLAC3D can reproduce the laminated roof failure in underground coal mines.

Keywords Coupled FDM-DEM · Underground coal mine · Laminated roof fracturing · Discontinuity strength

1 Introduction

Roof fall has been troubling underground mining industry for decades and caused numerous fatalities worldwide [1, 2]. Laminated roof, which is present in almost every underground coal mine in the USA, served as a key contributor to roof falls, especially cutter roof failure [1]. Laminated roof is distinct from regular roof rocks due to the existence of abundant parallelly distributed discontinuities. A lot of effort has been expended to study the influential factors of laminated roof stability, such as in situ stress [3, 4], mechanical properties of the roof [5, 6], and their solution through various methods, e.g., experimental methods, field observation, and numerical methods. However, the fracturing process in a laminated roof of underground entries and the effect of discontinuities have not been studied. This research investigates these two topics.

In most numerical studies on roof falls, continuum-based numerical methods have been adopted to gain an understanding of roof fall [3, 7, 8]. Nevertheless, it has been revealed that oversimplified assumptions in these methods were used as the roof rocks (i.e., shale or sandstone) consist of fine grains with granular behavior. The oversimplicity could cause roof behavior to be modeled under unrealistic conditions [5, 9, 10]. Furthermore, the large deformation and

---

✉ Qingwen Shi
wvuqingwenshi@gmail.com

[1] Department of Mining Engineering, West Virginia University, Morgantown, WV 26505, USA

[2] Department of Mining Engineering, The University of Utah, Salt Lake City 84112, USA

fracture propagation are difficult to be interpreted in continuum approaches.

The discrete element method explicitly takes into account the discrete nature of granular material that makes up the roof [11, 12]. This method, well developed in the past decades, has been widely employed in roof fall studies [5, 9, 10] For example, Gao [5] used both PFC and 3DEC to investigate the effect of horizontal stress on roof fracturing behavior. The cutter roof failure was also observed. Their research shows that the DEM is capable of reproducing the stress and deformation characteristics in the field. However, the main limitation with DEM also arises from its nature of discrete characteristics. When studying large-scale engineering problems, the DEM requires handling a large number of discrete elements to represent the whole structure, sometimes resulting in unaffordable computation time.

In the past few years, the coupling of discrete and continuous approaches emerged as a promising alternative for the improvement of numerical models. In this approach, the DEM is used in the area of interest, while the continuum approach is used in the far-field that is out of the researchers' interest. Through this coupling strategy, the computational time can be reduced without sacrificing the accuracy of the calculated results, making it possible to study a specific topic of a large model. However, the application of the coupled method in underground coal mines is still rare. In addition, no reported application with respect to the laminated roof study was found. Among these few attempts, Huo et al. [13] modeled the top coal caving with PFC3D and FLAC3D. Zhang et al. [14] simulated the overburden strata movement and near-surface stress change of a longwall coal mine using coupled 3DEC and FDM. Their comparison with results of continuum modeling shows that the coupled method appears to be more rigorous.

In this research, we created a coupled finite difference method (FDM)/discrete element method (DEM) model to investigate the fracturing behavior of the laminated roof of a mine entry. The laminated roof is created by bonded particle material with PFC3D, which is calibrated based on laboratory tests on the synthetic laminated rock. The surrounding rock including ribs and floor are created with finite zones with FLAC3D.

2 Methodology

2.1 Coupled FDM-DEM Working Mechanism

In the coupled method, the accuracy is ensured by the interaction that occurs in the interface between DEM particles in PFC3D and FDM zones in FLAC3D [11], as shown in Fig. 1. The interface serves as a boundary condition for both the DEM domain and the FDM domain. The DEM particle acts as a stress/force boundary of the FDM zones. Both contact forces and moments of DEM particles are transferred to the FDM elements through the contact point within the interface. Meanwhile, the FDM gridpoint velocities within the interface are calculated every time step and transferred to the DEM particle. In the Itasca software, this vital process is realized by wall-zone logic. The critical time step needs to be identical in both the DEM domain and FDM domain to ensure data exchange.

In this wall-zone logic, the gridpoint coordinates are captured and transferred into DEM wherein wall facets are created to wrap these FDM zones. The wall facets are responsible to interact with particle force/moments and gridpoint velocities. Every time step, the gridpoint coordinates are renewed; the wall facets are renewed accordingly; hence, the velocity boundary applied to the discrete particles can be updated. Similarly, the discrete force and moments passed to the gridpoints by the wall facets are updated simultaneously. In this scheme, quadrilateral zone faces are broken into two triangles [15]. Forces are calculated for the three gridpoints corresponding with the wall facet. When a particle is in contact with a triangular wall facet which is created to wrap a zone face, we denote the position of the closest point on the wall facet to the contact point as a vector $\overrightarrow{CP}$, as shown in Fig. 2. In the wall-zone logic, a barycentric interpolation/extrapolation is adopted to extrapolate values of this

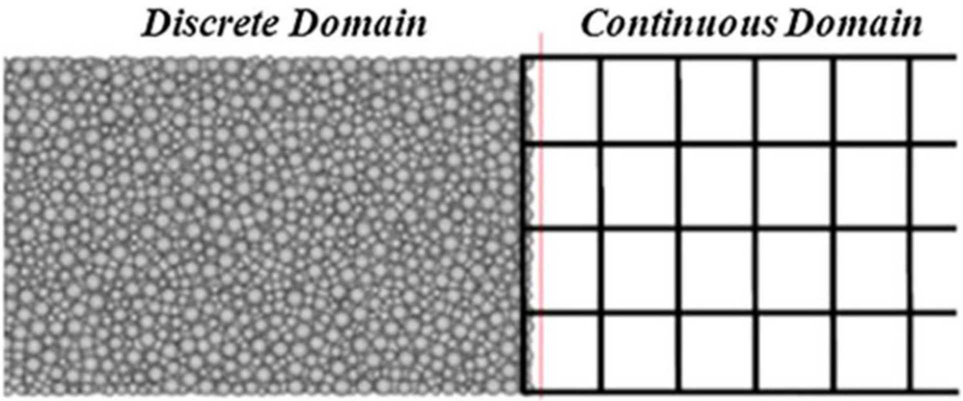

Fig. 1 Interaction approach between discrete particles and continuous domain (modified from [11])

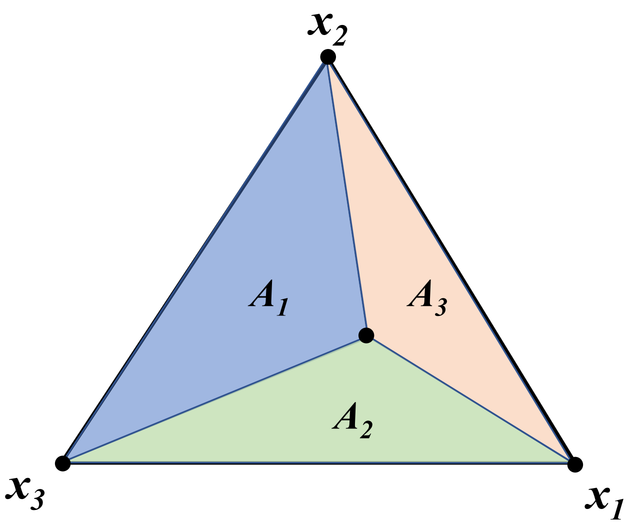

Fig. 2 Depiction of barycentric interpolation scheme [15]

point (forces and moments) to the vertices of the triangle, which coincide with the zone gridpoints. $\overrightarrow{X_i}$, $i = 1,2,3$, represents the locations of the three triangular vertex. Therefore, weighting factors are determined for each vertex by taking the triangle area opposite a vertex divided by the total area of the triangle, i.e., $w_i = A_i/A$. Thus, each value of the CP can be passed to the vertex by the derived weighting factors.

2.2 Modeling Procedure of the Entry Model with Coupled PFC3D/FLAC3D

The coupled numerical models consist of three components: continuum zones, bonded particle material (BPM) representing intact roof, and discontinuities in the laminated roof. The modeling procedures consist of four steps:

2.2.1 Creation of FDM Geometry

In the coupled model, the model geometry based on a longwall coal mine in the eastern US reported by Esterhuizen et al. [16]. The Pocahontas No. 3 seam is extracted in this coal mine. Sandstones and bedded shales are commonly observed in the overburden, as shown in Fig. 3a. The mining height averages 2.3 m, and the entry width averages 6.0 m. The coal seam thickness varies and is slightly smaller than the mining height. The model is set with a width of 30 m and a length of 30 m. The dark gray shale and sandy fireclay in Fig. 3a are treated as one stratum. The four strata on the top of Fig. 3a are also taken as one stratum since the interbedding, including gray shale and laminated sandstone, is thin or even not present at times. Also, the coal seam thickness is set the same as the mining height, which is 2.3 m. Therefore, an FDM model with dimensions of 30×30×18 m is created, as shown in Fig. 3b. The FDM model is created and equilibrated under the in situ stress during this step. The in situ stress is set according to the reported data [17] and discussed in the section that follows.

2.2.2 Generation of BPM

The objective of this PFC3D/FLAC3D coupled model is to investigate the roof failure behavior. Therefore, DEM particles are only applied to the immediate shale roof as shown in Fig. 4.

The length of the BPM is set smaller than that of the FDM model, with an ultimate dimension of 10×3×27 m. To realize the DEM particle generation, the zones in the targeted location are nulled, and then wall facets are

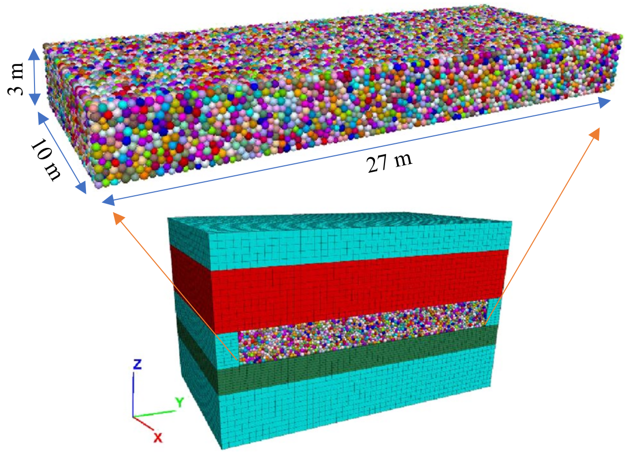

Fig. 4 Generation of the BPM in the FDM domain

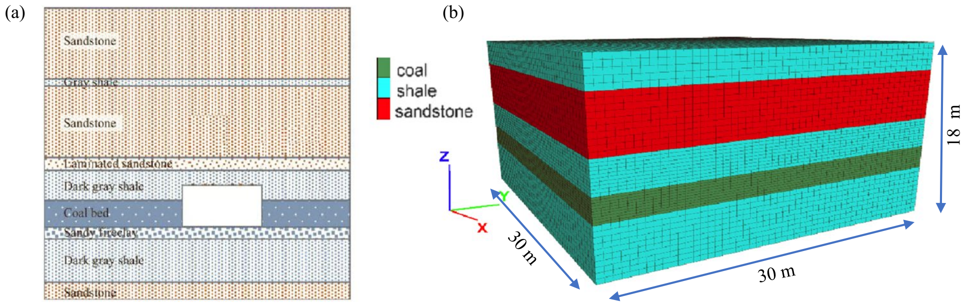

Fig. 3 The profile of the strata of **a** the test mine (modified from Esterhuizen et al. [16]) and **b** the created FDM model

created at the surface of nulled zones. The BPM is equilibrated after it is generated. During this equilibrating process, the wall facets are fixed to ensure the interaction is not activated at this stage. In other words, the equilibrating process of the BPM is independent of the FDM zones.

2.2.3 Installation of Parallel Discontinuities in the BPM

Three parallel discontinuities are installed in the BPM roof to simplify the model, which means the spacing of the discontinuities is 1.0 m. The realization of the discontinuities is achieved using the provided smooth joint logic [15, 18] in PFC3D. In the smooth joint model, the particle pair is intersected by a smooth joint to overlap and pass through each other instead of moving around one another model. This method is easy to use; however, the joint face may have inestimable roughness because of the interlock between particles on the joint face [19].

Once the installation of parallel discontinuities is completed, the wall facets are set free and the BPM with discontinuities interacts with the FDM zones through the wall facets and the coupled model is finally equilibrated under the in situ stress.

2.2.4 Stage-by-Stage Excavation of the Entry

The entry excavation with a dimension of 6.0 × 2.3 m is then simulated by nulling the FDM zones. To avoid unstable model response and ensure realistic excavation simulation, we advanced the entry by an incremental stage of 1.2 m. The advancing is set in the *Y* direction, as shown in Fig. 5.

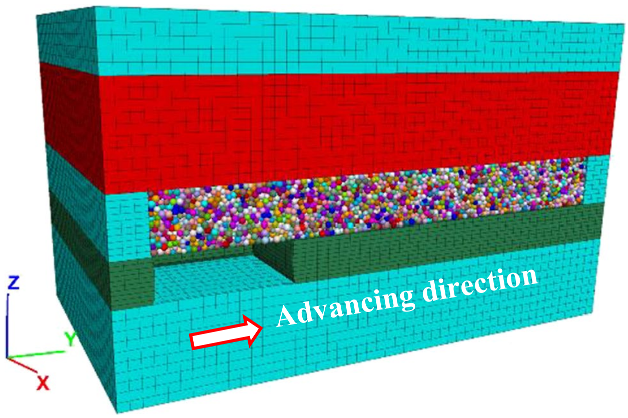

Fig. 5 Schematic diagram of the advancing entry

3 Model Setup and Calibration

3.1 Set Up of the FDM Model

As mentioned earlier, the coupled model typically simulates a horizontal extent of 30 m by 30 m. The Pocahontas No. 3 seam overburden depth in the test coal mine varies from 430 to 731 m [16]. Stress measurements conducted at the mine indicated maximum horizontal stress of approximately 21.1 MPa (σ_x) oriented at N58E, and a minor horizontal stress of approximately 13.9 MPa (σ_y). According to the layout of the entry, the angle (α) between the orientation of the maximum stress and the longitudinal axis of the test entry is approximately 45°, as shown in Fig. 6.

Therefore, the horizontal normal and shear stresses are resolved to the model boundary as follows [20]:

$$\sigma_\alpha = \frac{\sigma_x + \sigma_y}{2} + \frac{\sigma_x - \sigma_y}{2}\cos 2\alpha - \tau_x \sin 2\alpha = 8.6\mathrm{MPa} \tag{1}$$

$$\tau_\alpha = \frac{\sigma_x - \sigma_y}{2}\sin 2\alpha + \tau_x \cos 2\alpha == 3.6\mathrm{MPa} \tag{2}$$

The vertical stress is set as 12.0 MPa, corresponding to the depth of 500 m.

3.2 Calibration of Laminated BPM

Laboratory test data of synthetic laminated rocks is used for laminated BPM calibration in the coupled model. The synthetic laminated rocks are made of a mixture of Portland cement, sand, and hydrated lime with a ratio of Portland cement:sand:hydrated lime:water = 1.0:0.8:0.2:0.55. The mixture is poured layer by layer to reproduce laminated material in the laboratory. After the synthetic laminated rocks were cured, we prepared them into standard discs with a diameter of 54 mm, as per ASTM standard [21], for the

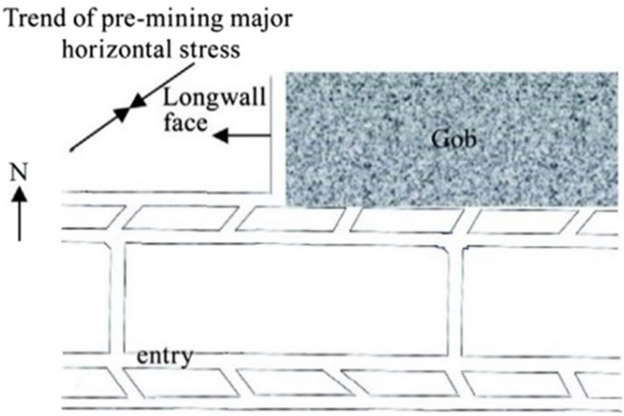

Fig. 6 Direction of the entries and the horizontal stresses [16]

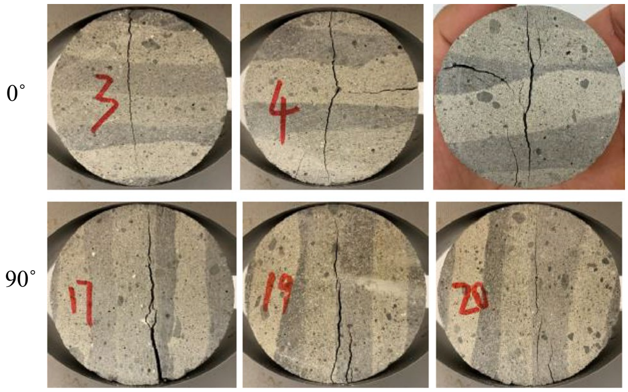

Fig. 7 Typical failure modes of the synthetic laminated rocks

Brazilian test. The tests are conducted with lamination orientations of 0° and 90°, respectively, as shown in Fig. 7. Results show that the tensile strength of discs oriented at 0° averaged 2.3 MPa, while that oriented at 90° averaged 1.8 MPa.

There is no efficient way to calibrate the BPM having parallel discontinuities. Researchers have to adjust the micro-parameters through trial and error, based on observation of the failure mode and failure strength. We have to note that the laboratory test results have to be scaled when they are applied to large-scale rock mass during the calibration. In the present research, the strength reduction factor of 0.58 [22] is used for the BPM with discontinuities. The calibrated micro-parameters, including BPM and discontinuities, are shown in Tables 1 and 2.

With the combination of micro-parameters illustrated in Tables 1 and 2, the calibrated laminated BPM discs show Brazilian tensile strength values of 1.15 MPa and 0.95 MPa for discs orientated at 0° and 90°, respectively, which are close to the scaled strength of 1.15 MPa and 0.92 MPa. Furthermore, Fig. 8 illustrates the failure pattern of the numerical Brazilian discs. The green part represents the particles and the red flakes represent the fractures in the discs. It can be concluded that the numerical failure pattern agrees well with the laboratory test results.

Table 1 Micro-parameters of rock matrix used in the BPM

Micro-parameter	Value
Particle density, kg/m^3	2500
Particle size, m	0.10 to 0.15
Bond gap, m	6.0×10^{-5}
Young's modulus of the particle, GPa	0.48
Young's modulus of the parallel bond, GPa	0.48
Ratio of normal to shear stiffness of the particle	1.0
Ratio of normal to shear stiffness of the parallel bond	1.0
Particle friction coefficient	0.7
Parallel bond tensile strength, MPa	0.38
Parallel bond cohesion, MPa	2.4
Friction angle, degree	31

Table 2 Micro-parameters of parallel discontinuities installed in the BPM

Micro-parameter	Value
Normal stiffness of smooth joint, GPa	100
Shear stiffness of smooth joint, GPa	200
Tensile strength of smooth joint, GPa	1.68
Shear strength of smooth joint, MPa	24.0
Friction coefficient	0.6
Contact gap, m	6.0×10^{-3}

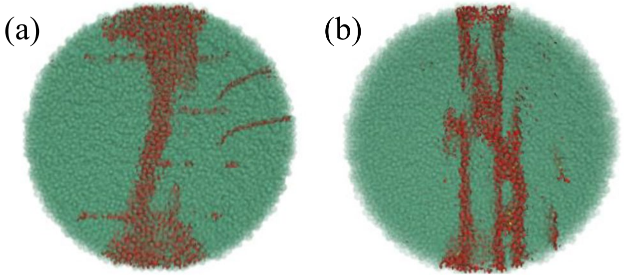

Fig. 8 Failure pattern of the numerical discs oriented at **a** 0° and **b** 90°

4 Comparison of the Laminated Roof and Intact Roof

With the coupled model created above, we analyzed the failure behavior between the laminated roof and intact roof to demonstrate the effect of parallel discontinuities in the immediate roof.

4.1 Roof Displacement Comparison

After the entry excavation, we captured the maximum roof displacement in a cross Sect. 1.8 m behind the driving face, as shown in Fig. 9. The maximum roof displacement in the intact roof model is 0.21 m, while this value in the laminated roof model is 0.23 m. Additionally, the displacement distribution is different. Although the maximum displacement is smaller in the intact immediate roof model, the displacement is distributed in the whole BPM, which means the immediate roof converges as a whole. In contrast, the roof displacement dominantly takes place on the roofline in the laminated model. This indicates that the laminated roof deformation starts with the outer layers near the roof skin before failure.

4.2 Cracks and Contact Force Distribution Comparison

In BPM, the particles interact by contact forces at their contacting points. The contact forces can be readily depicted in

Fig. 9 Displacement distribution in **a** the intact roof model and **b** the laminated roof model

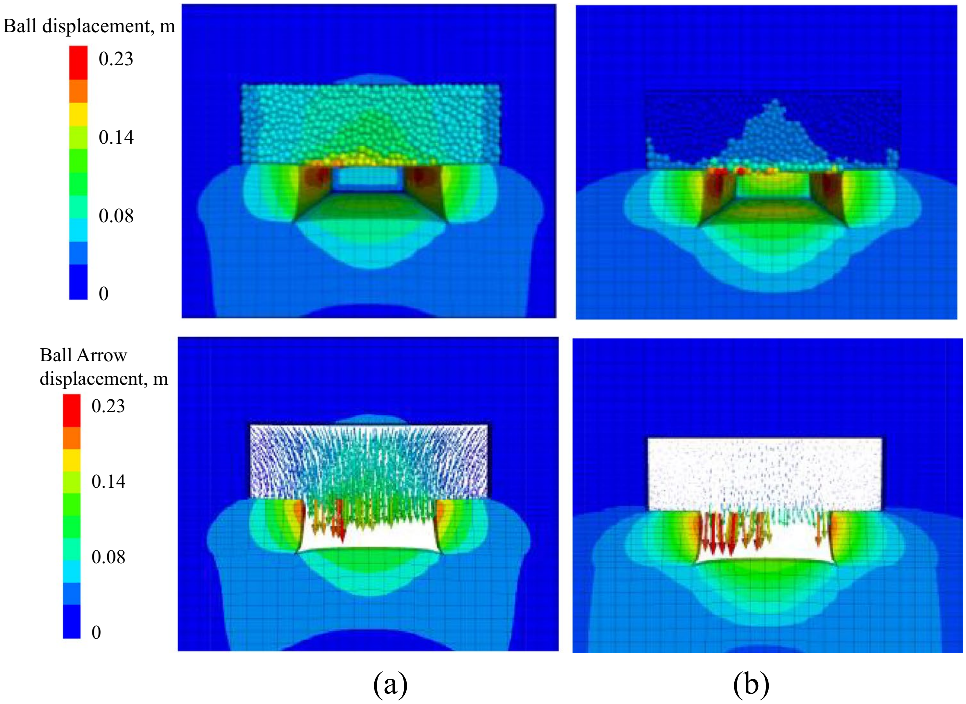

PFC3D. The contact force field in both the intact roof model and laminated roof model is illustrated in Fig. 10, where the compressional and tensile contacts forces are displayed by green and red cylinders, respectively, with diameters indicative of the force value. The faded cylinders in the contact force field represent failed bonds between the particles.

By comparison, it can be observed that the roofline of the laminated model loses its contact force thoroughly while that of the intact roof model only fades slightly, indicating that the surface of the laminated roof loses its self-supporting capacity due to the discontinuities inside the roof. Additionally, at some locations where the discontinuities are installed, the tensile forces were observed, indicating a relatively unstable roof.

4.3 The Number and Distribution of Cracks Comparison

The resulting cracks obtained from the intact roof and laminated roof are presented in Fig. 11. We observed that the crack distribution pattern in the intact roof model is characterized by a dome shape, while the laminated model cracks appear by layers in a horizontal orientation. This proved the effect of the lamination on the roof failure.

As can be seen in the laminated model in Fig. 11b, the cracks develop along with but are not limited to the installed discontinuities. The bottom layer of the laminated roof is fractured thoroughly and the middle two layers remain intact. However, the discontinuities between these two layers are fractured, as illustrated by the cracks located along the discontinuities.

Through the comparison of displacement, contact force field, and crack distribution of intact roof model and laminated roof model, we generally conclude that the lamination imposes a pronounced effect on the roof failure, which agrees well with common knowledge.

Fig. 10 Contact force field in **a** intact roof model and **b** laminated roof model

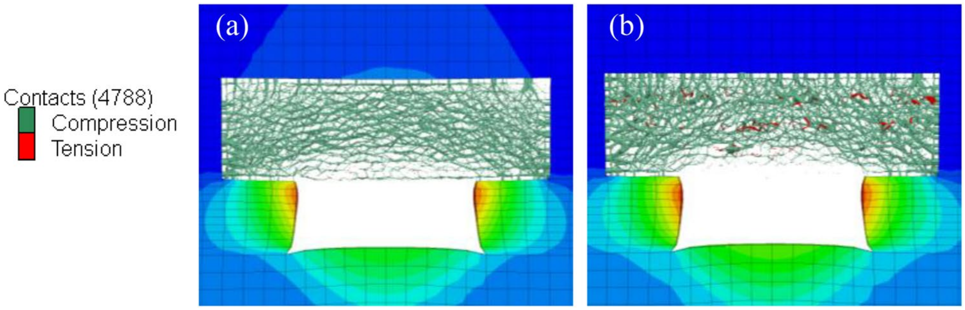

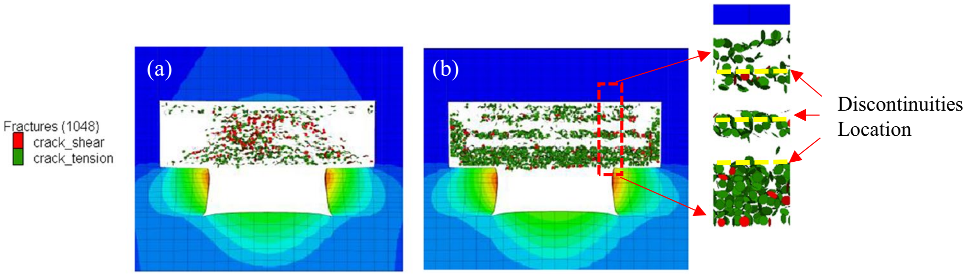

Fig. 11 The crack distribution of **a** the intact roof model and **b** the laminated roof model

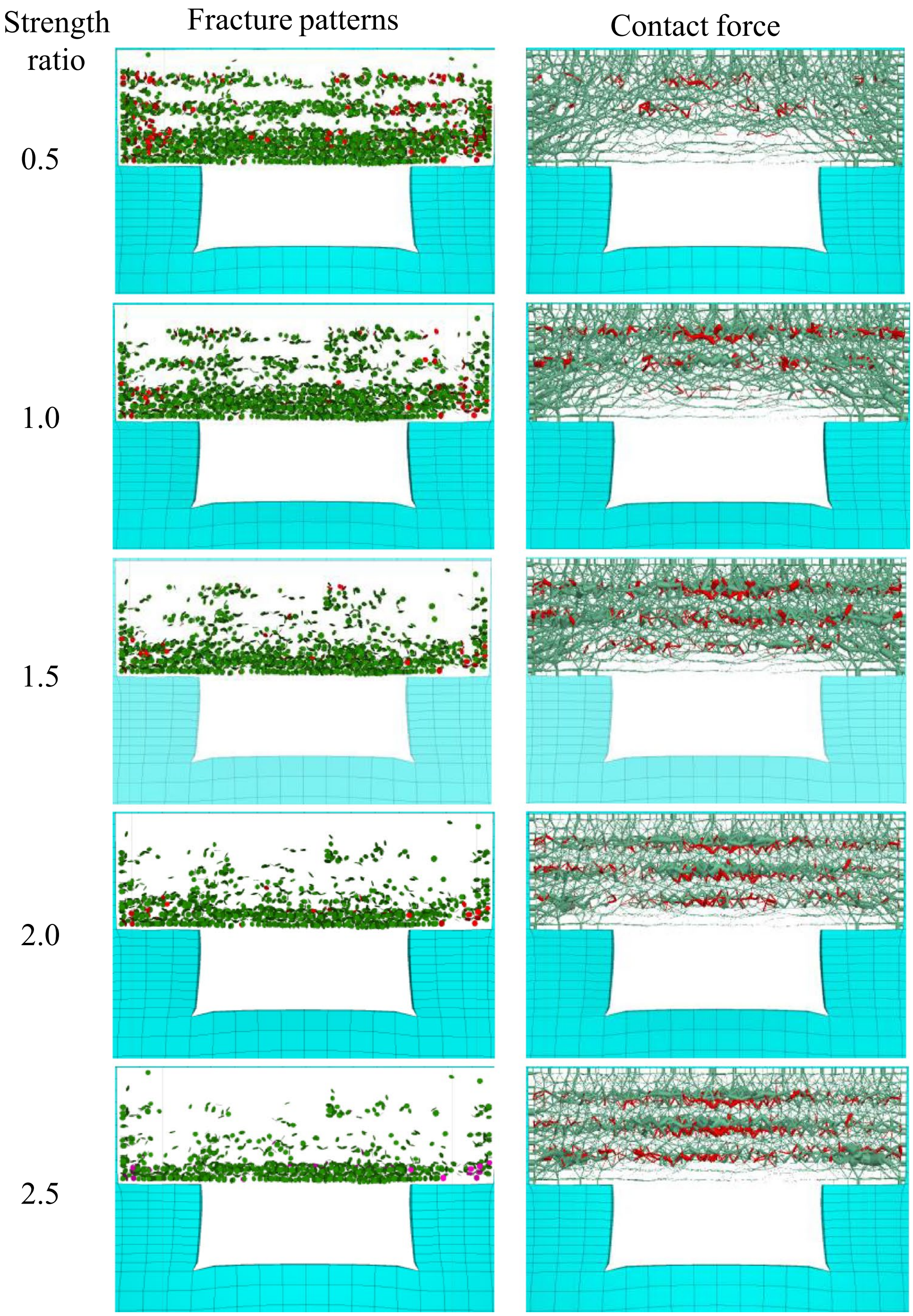

Fig. 12 Fracture patterns and contact force distribution

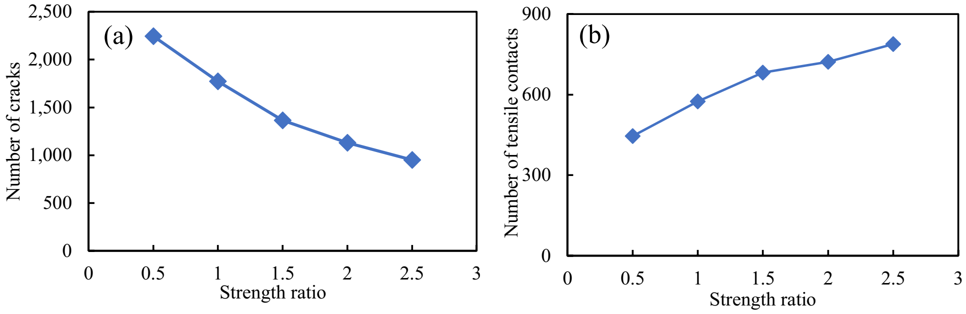

Fig. 13 Number of **a** total cracks and **b** tensile contacts in the cross section

5 Effect of Discontinuity Strength on Laminated Roof Failure

To investigate the sensitivity of the roof failure to the discontinuity strength in the laminated model, the strength of the discontinuities was varied by changing the smooth joint strength at different ratios. The strength ratio was varied to 0.5, 1.0, 1.5, 2.0, and 2.5, respectively. All other parameters in the numerical model were kept constant. At different models, the fracture patterns, contact force field, and crack distribution of the laminated roof with respect to entry advance are discussed.

5.1 Fracture Patterns and Contact Force Field

Figure 12 shows the fracture patterns and contact force distribution in models with various plane strengths in a cross section. The signs and their physical meanings are the same as in earlier sections.

We observed a difference in both crack distribution patterns and the size of the distribution range in various models. In models with a lower strength ratio, cracks are characterized by distribution in both the roofline and along the discontinuities, as shown in models with a strength ratio of 0.5 and 1.0 in Fig. 12. This distribution along the discontinuities fades when the strength ratio increases. When the strength ratio reaches 2.5, most fractures are only distributed on the roofline, i.e., the outer layer near the roof skin of the laminated roof.

We observe a faded area of contact force on the roofline in every model, which formed a force arch in the laminated roof, as shown in Fig. 12. This phenomenon is most noticeable in the model with a strength ratio of 0.5. However, the scale of the faded area decreases with an increase in the strength ratio, demonstrating that the failed depth of the laminated roof decreases when the discontinuity strength increases. Additionally, tensile contacts are observed where the discontinuities are located, which implies a different failure mechanism between discontinuities and intact layers.

Figure 13a shows the total number of cracks against the strength ratio of discontinuities, demonstrating that the number of cracks in the laminated roof decreases monotonically with an increment of discontinuity strength. Figure 13b plots the number of tensile contacts against the discontinuity strength ratio, demonstrating a monotonical increment of tensile contacts with strength ratio. This is because the tensile contacts in models with lower strength ratios are debonded more easily than those with higher strength ratios, which is validated by the pictures of fracture patterns, wherein models with lower strength ratios presented more fractures along the discontinuities.

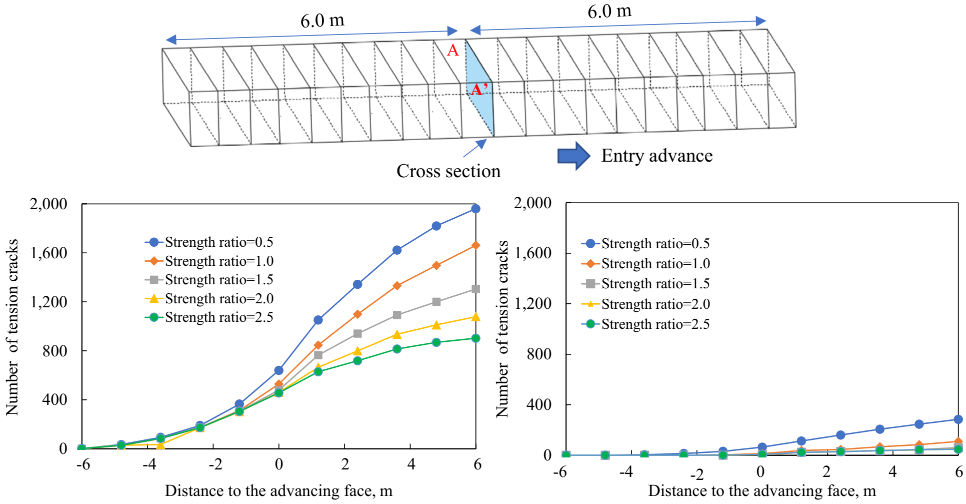

Fig. 14 The relationship between entry advance, the strength ratio, and the number of **a** tension cracks and **b** shear cracks developed in the laminated roof

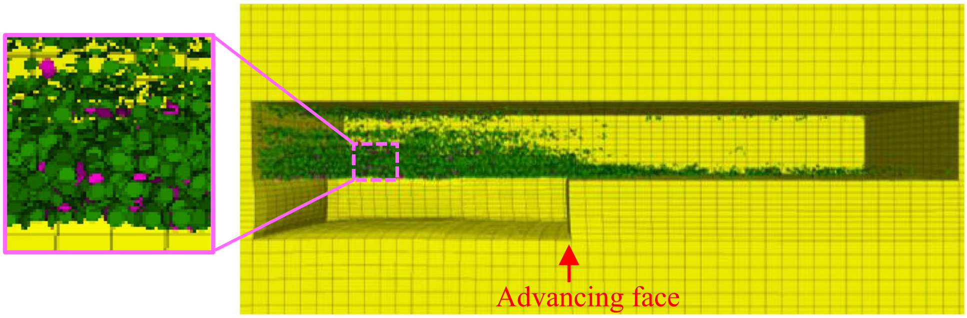

Fig. 15 The 3D diagram of crack distribution with respect to the advancing face

5.2 Crack Propagation with Entry Advance

Entry advance introduces changing stress conditions on the surrounding rock [23], which poses an effect on the fracturing behavior of the roof. Coupled FDM and DEM model enables us to monitor the number of cracks developed in the model through either tension or shear with entry advance. To observe the difference of advancing face's effect on the laminated roof, only cracks in the cross section located at the middle of the model are monitored. Figure 14 shows the relationship between entry advance, the strength ratio, and the number of both shear and tension cracks developed in the laminated roof. The negative values in the *X*-axis mean that the monitoring cross section is ahead of the advancing face, while the positive values represent the distance the cross section behind the advancing face.

We observed in both Fig. 14a and b that the numbers of both shear and tension cracks increase as the entry advances in all the models. In each case, tension cracking consistently exceeds shear cracking by a ratio of 6.9 or higher. For a fixed distance to the advancing face in both figures, the tension cracks and shear cracks exhibit a similar trend as the strength ratio increases. In general, the number of both shear and tension cracks decreases as the strength ratio increases. The maximum value of both shear and tension cracks occurs when the strength ratio is 2.5, reflecting the optimum stability of the laminated roof when the discontinuity strength is largest. The models with low discontinuity strength suffer more fracturing than those with high discontinuity strength. The numerical results agree well with the reported research on the sensitivity analysis of interfaces in laminated rocks [24].

Figure 15 depicts the crack distribution induced by the entry excavation in a 3D view. The green flakes correspond to the tensile cracks, while the red ones correspond to the shear cracks. It is illustrated that the tensile cracks are significantly more than shear cracks in quantity, validating the conclusion drawn from Fig. 14. In addition, cracks are distributed in both the roof behind the advancing face and ahead of the advancing face. Based on the simulation, the cracks induced by the excavation can extend 15 m ahead of the advancing face in the laminated model.

We extracted the crack distribution ahead and behind the advancing face, respectively. Figure 16 shows the number of cracks behind and ahead of the advancing face, respectively, illustrating that the trend of the crack number of all the models is generally similar. The number of cracks in each model is linearly positive to the advancing footage of the entry. The cracks behind the advancing face increase with a decrease in the discontinuity strength. However, this trend is sensitive to the strength ratio, which can be demonstrated by the crack number increment between different strength ratios. When the strength ratio decreases at a fixed interval of 0.5, the increment of crack numbers gets larger. For example, at the footage of 21 m, the crack number differences between each strength ratio of 2.5 and 2.0, 2.0 and 1.5, 1.5 and 1.0, 1.0 and 0.5 are observed as 5506, 9475, 13,759, and 14,588, respectively.

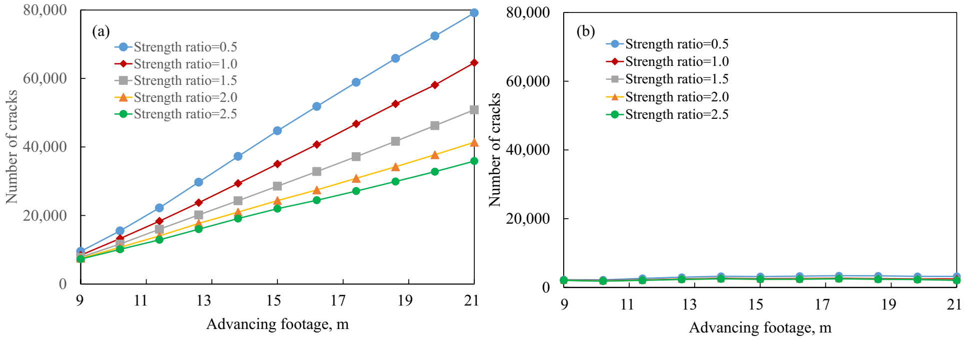

Fig. 16 Number of cracks **a** behind the advancing face and **b** ahead of the advancing face with respect of entry advance

Figure 16b demonstrates that though the crack extends a long distance ahead of the face, the number of cracks ahead of the face remains relatively small in comparison to that behind the face. Additionally, this trend does change with the strength ratio of the discontinuity in the laminated roof, demonstrating that the strength ratio of discontinuity poses little influence on the roof fracturing ahead of the advancing face.

6 Conclusion

In the present study, a coupled FDM-DEM was used to investigate the laminated roof failure in an eastern coal mine in the USA. The laminated roof was simulated using bond particle material within the FEM domain realized by PFC3D. The parallel discontinuities were installed into the bonded particle material to reproduce the laminated roof. The micro-parameters were calibrated using Brazilian test results of synthetic laminated rock. The rest part of the coupled model was simulated using continuum zones within the FDM domain realized by FLAC3D. Four steps are adopted sequentially to complete the coupled method.

A comparison between the laminated roof and the intact roof was conducted. The results show that not only the laminated roof converges more but also the laminated roof failure initiates at the outer layer near the roof skin. Furthermore, the crack distribution in the intact roof is characterized by a dome shape, while the cracks are distributed along the discontinuities, which is consistent with the reported study. The fracturing process analysis was conducted using models with varying discontinuity strength. Increasing the discontinuity strength can change the crack distribution by increasing the tensile contact in the laminated roof. In addition, the discontinuity strength poses little influence on the roof fracturing ahead of the advancing face in comparison with that behind the face. The number of cracks during excavation decreases with the increment of discontinuity strength. But this trend gets more pronounced when the discontinuity strength is low. These results show that the coupled method using PFC3D/FLAC3D can reproduce the laminated roof fracturing process in underground coal mines.

Author Contribution Conceptualization and investigation, formal analysis, and writing (original draft), Qingwen Shi; funding acquisition and writing (review and editing), Brijes Mishra.

Funding This work was supported by the National Institute for Occupational Safety and Health (NIOSH) (No. 200–2016-92214).

Data Availability Not applicable.

Code Availability Not applicable.

Declarations

Conflict of Interest The authors declare no competing interests.

References

1. GS Esterhuizen TS Bajpayee (2012) Horizontal stress related failure in bedded mine roofs - insight from field observations and numerical models. Paper presented at the 46th US Rock Mechanics / Geomechanics Symposium, Chicago, Illinois, pp 68–77
2. Molinda G, Mark C (2010) Ground failures in coal mines with weak roof. Electron J Geotech Eng 15(1):42
3. Gadde MM (2004) Effect of in-situ stresses on the stability of coal mine development workings. Paper presented at the 23rd International Conference on Ground Control in Mining, Morgantown, West Virginia, pp 92–102
4. Xue Y, Mishra B (2015) Underground mine roof crack formation simulation with creep of rock mass. Paper presented at the *49th US Rock Mechanics / Geomechanics Symposium,* San Francisco, California, pp 2392–2397
5. Gao F, Stead D (2013) Discrete element modelling of cutter roof failure in coal mine roadways. Int J Coal Geol 116–117:158–171. https://doi.org/10.1016/j.coal.2013.07.020
6. Garg P (2018) Behaviour of laminated roof under high horizontal stress, West Virginia University, Dissertation. https://doi.org/10.33915/etd.7178
7. Shi Q, Xu G, Wang D, Li Z, Liu W, Wang X (2021) Chain pillar optimization at a longwall coal mine based on field monitoring results and numerical model analysis. Arab J Geosci 14(23):1–8. https://doi.org/10.1007/S12517-021-08843-0
8. Zipf RK (2006) Numerical modeling procedures for practical coal mine design. Paper presented at the 41st U.S. Symposium on Rock Mechanics (USRMS), Golden, Colorado
9. Abousleiman R, Walton G, Sinha S (2020) Understanding roof deformation mechanics and parametric sensitivities of coal mine entries using the discrete element method. Int J Min Sci Technol 30(1):123–129. https://doi.org/10.1016/j.ijmst.2019.12.006
10. Sherizadeh T, PHSW (2016) Kulatilake, Assessment of roof stability in a room and pillar coal mine in the U.S. using three-dimensional distinct element method. Tunn Undergr Sp Technol 59:24–37. https://doi.org/10.1016/j.tust.2016.06.005
11. Breugnot A, Lambert S, Villard P, Gotteland P (2016) A discrete/continuous coupled approach for modeling impacts on cellular geostructures. Rock Mech Rock Eng 49(5):1831–1848. https://doi.org/10.1007/s00603-015-0886-8
12. Cundall PA (1971) A computer model for simulating progressive large-scale movements in blocky rock systems. Presented at the Proceedings of the International Symposium on Rock Mechanics, Nancy, France
13. Huo Y, Song X, Zhu D (2020) Numerical investigation of top-coal migration in the first coal-drawing process by an FDM–DEM coupling method. Energies 13(20):5493. https://doi.org/10.3390/en13205493
14. Zhang P, Gearhart D, Van Dyke M, Su D, Esterhuizen E, Tulu B (2019) Ground response to high horizontal stresses during longwall retreat and its implications for longwall headgate support. Int J Min Sci Technol 29(1):27–33. https://doi.org/10.1016/j.ijmst.2018.11.020
15. Itasca (2019) PFC Version 5.0. Itasca Consulting Group Inc., Minneapolis, Minnesota
16. Tulu IB, Esterhuizen GS, Mohamed KM, Klemetti TM (2017) Verification of a calibrated longwall model with field

measurements. Paper presented at the 51st U.S. Rock Mechanics/Geomechanics Symposium, San Francisco, California

17. Esterhuizen GS, Gearhart DF, Klemetti T, Dougherty H, van Dyke M (2019) Analysis of gateroad stability at two longwall mines based on field monitoring results and numerical model analysis. Int J Min Sci Technol 29(1):35–43. https://doi.org/10.1016/j.ijmst.2018.11.021
18. Shi Q, Mishra B (2021) Discrete element modeling of delamination in laboratory scale laminated rock, *Mining*. Metall Explor 38(1):433–446. https://doi.org/10.1007/s42461-020-00302-w
19. Shi Q, Mishra B, Zhao Y (2022) DEM analysis of the effect of lamination properties on the stability of an underground coal mine entry with laminated shale roof, *Mining*. Metall Explor 2022:1–12. https://doi.org/10.1007/S42461-022-00541-Z
20. Boresi AP, Schmidt RJ (1985) Advanced Mechanics of Materials. Fourth Edition, New York
21. ASTM Standard D3967-16 (2016) Standard test method forsplitting tensile strength of intact rock core specimens.ASTM International, West Conshohocken, USA
22. Gadde M, Rusnak J, Honse J, Peng SS. On rock failure criteria for coal measure rocks. Presented at 26th International Conference on Ground Control in Mining. Morgantown, West Virginia, pp 361–369
23. Shi Q, Pan J, Wang S, Liu S, Mishra B, Seitz S (2021) Field monitoring of delayed coal burst in an advancing entry of a deep coal mine, *Mining*. Metall Explor 2021:1–15. https://doi.org/10.1007/S42461-021-00508-6
24 Zhang K, Yang T, Bai H, PathegamaGamage R (2018) Longwall mining–induced damage and fractures: field measurements and simulation using FDM and DEM coupled method. Int J Geomech 18(1):04017127. https://doi.org/10.1061/(ASCE)GM.1943-5622.0001040
25. Clifford B (2004) The assessment of ground control risk and support integrity in coal mine roadways, University of Exeter, Dissertation
26. Cundall PA, Strack ODL (1979) A discrete numerical model for granular assemblies. Géotechnique 29(1):47–65. https://doi.org/10.1680/geot.1979.29.1.47